1   Hysteric temperature sensitivity of wetland CH$_4$ fluxes explained by substrate

2   availability and microbial activity

3   Kuang-Yu Chang*,

4   Climate and Ecosystem Sciences Division, Lawrence Berkeley National Laboratory,

5   Berkeley, California, USA

6   William J. Riley,

7   Climate and Ecosystem Sciences Division, Lawrence Berkeley National Laboratory,

8   Berkeley, California, USA

9   Patrick M. Crill,

10   Department of Geological Sciences and Bolin Centre for Climate Research, Stockholm

11   University, Stockholm, Sweden

12   Robert F. Grant,

13   Department of Renewable Resources, University of Alberta, Edmonton, Alberta, Canada

14   Scott R. Saleska

15   Department of Ecology and Evolutionary Biology, University of Arizona, Tucson,

16   Arizona, USA

17   *Corresponding author: Kuang-Yu Chang, ckychang@lbl.gov

18   Climate and Ecosystem Sciences Division, Lawrence Berkeley National Laboratory

19   Berkeley, California, USA

20   Phone: (510) 495-8141

21   Key words: Methane cycling; microbial dynamics; climate change; IsoGenie Project;

22   Stordalen Mire

Abstract

Methane (CH_4) emissions from wetlands are likely increasing and important in global climate change assessments. However, contemporary terrestrial biogeochemical model predictions of CH_4 emissions are very uncertain, at least in part due to prescribed temperature sensitivity of CH_4 production and emission. While statistically consistent apparent CH_4 emission temperature dependencies have been inferred from meta-analyses across microbial to ecosystem scales, year-round ecosystem-scale observations have contradicted that finding. Here, we show that apparent CH_4 emission temperature dependencies inferred from year-round chamber measurements exhibit substantial intra-seasonal variability, suggesting that using static temperature relations to predict CH_4 emissions is mechanistically flawed. Our model results indicate that such intra-seasonal variability is driven by substrate-mediated microbial and abiotic interactions: seasonal cycles in substrate availability favors CH_4 production later in the season, leading to hysteretic temperature sensitivity of CH_4 production and emission. Our findings demonstrate the uncertainty of inferring CH_4 emission or production rates from temperature alone, and highlight the need to represent microbial and abiotic interactions in wetland biogeochemical models.

1. Introduction

Methane (CH_4) is the second most important climate forcing gas with at least a 28-fold higher global warming potential (GWP) than carbon dioxide (CO_2) over a 100-year horizon (Myhre, *et al* 2013). Atmospheric CH_4 concentrations have more than doubled since 1750 (Saunois et al., 2016) and have contributed about 20% of the additional radiative forcing accumulated in the lower atmosphere (Ciais et al., 2013). Recent assessments have found that CH_4 emissions from wetland and other inland waters are the largest and most uncertain sources affecting the global CH_4 budget (Kirschke et al., 2013; Poulter et al., 2017; Saunois et al., 2016). Such CH_4 emissions account for 25 to 32% of current global total CH_4 emissions (Saunois et al., 2016) and contribute substantially to the renewed and sustained atmospheric CH_4 growth after 2006 (Saunois et al., 2017). Increasing CH_4 emissions could offset mitigation efforts and accelerate climate change (Bastviken et al., 2011; Kirschke et al., 2013) due to their strong influence on the global radiative energy budget (Neubauer and Megonigal, 2015). However, CH_4 emission estimates are poorly constrained due to insufficient quality-controlled measurements (Bastviken et al., 2011; Kirschke et al., 2013; Saunois et al., 2016) and uncertain model structures and parameterizations (Melton et al., 2013; Wania et al., 2013; Xu et al., 2016). In fact, simulations in the ongoing Coupled Model Intercomparison Project Phase 6 (CMIP6; (Eyring et al., 2016)) do not even request wetland CH_4 emission predictions for the historical or 21st century periods. A number of knowledge gaps (Xu et al., 2016) need to be addressed to improve CH_4 model representations and thereby CH_4 climate feedback predictions (Dean et al., 2018). Such efforts are imperative because, among other reasons, permafrost degradation resulting from observed global-scale

64 permafrost warming (Biskaborn et al., 2019) can stimulate organic matter decomposition

65 (Schuur et al., 2015) that could augment global warming with a strong contribution from

66 CH_4 (Knoblauch et al., 2018).

67 Many contemporary terrestrial biogeochemical models parameterize CH_4

68 production (or even CH_4 emissions) as a static temperature function of net primary

69 production or heterotrophic respiration (Melton et al., 2013; Wania et al., 2013; Xu et al.,

70 2016). Such parameterization is supported by recent meta-analyses that indicate a static

71 and consistent apparent CH_4 production and emission temperature dependence across

72 microbial to ecosystem scales (Yvon-Durocher et al., 2014). However, measurements

73 collected across sites with nearly identical wetland climate, hydrology, and plant

74 community compositions suggest large spatial and temporal variability in the ratio

75 between ecosystem productivity and CH_4 emissions (Hemes et al., 2018). Further,

76 ecosystem-scale CH_4 emissions have hysteretic responses to seasonal changes in gross

77 primary productivity (GPP), water table depth (WTD), and temperature (Brown et al.,

78 2014; Goodrich et al., 2015; Rinne et al., 2018; Zona et al., 2016), suggesting that CH_4

79 biogeochemistry may not be accurately represented by static relationships. Consequently,

80 a mechanistic understanding of factors modulating CH_4 production and emission rates is

81 urgently needed to improve the currently uncertain CH_4 biogeochemistry

82 parameterization.

83 Although observations of changes in CH_4 production, oxidation, and emission

84 rates; spatial heterogeneity; and seasonal dynamics following permafrost degradation

85 have been discussed (Hodgkins et al., 2014; McCalley et al., 2014; Olefeldt et al., 2013;

86 Perryman et al., 2020), an understanding of mechanisms regulating intra-seasonally

87 varying CH_4 emissions and their response to temperature is still lacking. We therefore

88 investigated the impacts of soil thermal and hydrological history on CH_4 emissions to

89 improve understanding of apparent CH_4 emission temperature dependence and inform

90 CH_4 model structure and parameterization. We hypothesized that a static apparent CH_4

91 emission temperature dependence is not sufficient for modeling CH_4 emissions due to

92 substrate-mediated hysteretic microbial and abiotic interactions (Tang and Riley, 2014)

93 over seasonal time scales. We used a comprehensive biogeochemistry model (*ecosys*) to

94 investigate observed intra-seasonal changes in apparent CH_4 emission temperature

95 dependence at two high-latitude sites: Stordalen Mire (68.2 °N, 19.0 °E) and Utqiaġvik

96 (formerly Barrow, 71.3 °N, 156.5 °W). We focus most of the detailed analysis at

97 Stordalen Mire, where we recently validated the modeled CH_4 production pathways using

98 acetoclastic and hydrogenotrophic methanogen relative abundance inferred from 16S

99 rRNA gene amplicon sequencing data (Chang et al., 2019b). We also evaluated the

100 uncertainty of ignoring substrate-mediated hysteretic microbial and abiotic interactions.

101 **2. Methods**

102 **2.1 Study site description**

103 The Stordalen Mire sites are about 10 km east of the Abisko Scientific Research

104 Station in the discontinuous permafrost zone of northern Sweden and include intact

105 permafrost palsa, partly thawed bog, and fen (Hodgkins et al., 2014). The mean annual

106 air temperature and precipitation at the Stordalen Mire are around 0.6 °C and 336 mm y^{-1},

107 respectively. The measured CH_4 emissions are near zero in the palsa due to its deeper

108 WTD and shallower Active Layer Depth (ALD) (Bäckstrand et al., 2008b, 2008a, 2010);

109 we therefore did not include this site in our analysis. The bog is ombrotrophic (pH ~4.2)

with WTD fluctuating from the peat surface to 35 cm below the peat surface (Bäckstrand

et al., 2008b, 2008a; Olefeldt and Roulet, 2012), and is dominated by *Sphagnum* spp.

mosses with a moderate abundance of short sedges such as *Eriophorum vaginatum* and

Carex bigelowii (Bäckstrand et al., 2008b, 2008a; Malmer et al., 2005; Olefeldt and

Roulet, 2012). The fen is minerotrophic (pH~5.7), has WTD near or above the peat

surface throughout the growing season, and is dominated by tall sedges such as *E.*

angustifolium, *C. rostrata* and *Esquisetum* spp. (Bäckstrand et al., 2008b, 2008a; Olefeldt

and Roulet, 2012). The Stordalen Mire bog and fen both have a peat layer ranging from

0.5 to 1 m (Rydén and Kostov, 1980) and an ALD greater than 0.9 m (Bäckstrand et al.,

2008b).

The Utqiaġvik site is located at the Barrow Experimental Observatory at the

northern tip of Alaska's Arctic coastal plain, which is characterized by polygonal

landforms caused by seasonal freezing and thawing of tundra soil (Hinkel et al., 2005).

These polygonal landforms were categorized into separate features based on moisture

variation determined by surface elevations (Wainwright et al., 2015). We analyzed CH_4

emissions modeled in the low-centered polygonal landform that was represented as a

connected combination of trough, rim, and center structures (Grant et al., 2017b). The

mean annual air temperature and precipitation at Utqiaġvik are around -12°C and 106

mm y^{-1}, respectively. The ALD varies spatially from approximately 20 to 60 cm, which is

influenced by soil texture, vegetation, soil moisture, and inter-annual variability

(Shiklomanov et al., 2010).

2.2 Field measurements

132   A system of six automated gas-sampling chambers made of transparent Lexan

133   was installed at the Stordalen Mire in 2001 (three in the bog and three in the fen). Each

134   chamber covered an area of 0.14 m^2 (38 cm × 38 cm) with a height of 25–45 cm

135   depending on the vegetation and the depth of insertion, and was closed for 5 minutes

136   every 3 hours. In addition, each chamber is instrumented with thermocouples measuring

137   air and ground surface temperatures, and WTD is measured manually three to five times

138   per week from June to October each year (McCalley et al., 2014). The system was

139   updated with a new chamber design similar to that described in (Bubier et al., 2003) in

140   2011. The new chambers each cover an area of 0.2 m^2 (45 cm × 45 cm), with a height

141   ranging from 15 to 75 cm depending on habitat vegetation.

142   **2.3 Apparent temperature dependence calculation**

143   We quantify the apparent temperature dependencies of daily CH$_4$ emission and

144   CH$_4$ production by fitting Boltzmann-Arrhenius functions of the form:

145    $\ln F_i(T) = \overline{E_{a,\iota}} \cdot \left(\frac{-1}{kT}\right) + \varepsilon_{F_i}$ (Eq. 1)

146   where $F_i(T)$ is the rate of CH$_4$ emission (i = 1) and CH$_4$ production (i = 2) at absolute

147   temperature T. $\overline{E_{a,\iota}}$ (in eV) and ε_{F_i} correspond to the fitted apparent activation energy

148   (slope) and base reaction rate (intercept), respectively. k is the Boltzmann constant

149   (8.62 × 10^{-5} eV K^{-1}).

150   We defined earlier and later periods as the times before and after the highest daily

151   temperature analyzed in a given thawed season, respectively, to quantify intra-seasonal

152   changes in apparent CH$_4$ emission or production temperature dependencies. Thawed

153   seasons were defined as the time period when measured or modeled temperatures are at

154   least 1 °C to avoid low CH$_4$ emissions in the 0 − 1 °C temperature window that can alter

155 the base reaction rate of our Boltzmann-Arrhenius functions. Four types of temperature

156 were used in our analysis: (1) measured soil surface temperature (e.g., Fig. 1), (2)

157 modeled vertical mean 0 – 20 cm soil temperature (e.g., Fig. 2), (3) measured air

158 temperature (e.g., Supplementary Fig. 1), and (4) modeled air temperature (e.g.,

159 Supplementary Fig. 2). The vertical mean 0 – 20 cm soil temperature was chosen for our

160 analysis because CH_4 production at our study site is concentrated in the top 20 cm of soil

161 (Chang et al., 2019b). Consistent hysteretic temperature responses were derived with

162 above zero vertical mean 0 – 20 cm soil temperatures (i.e., include the modeled 0 – 1 °C

163 temperature window), e.g., Fig. 2 vs. Supplementary Fig. 3.

164 **2.4 Model description**

165   The *ecosys* model is a comprehensive biogeochemistry model that explicitly

166 represents interactions among biogeophysical (i.e., hydrological and thermal),

167 biogeochemical (including carbon, nitrogen, and phosphorus), plant and microbial

168 processes. The above-ground processes are represented in multi-specific multi-layer plant

169 canopies, and the below-ground processes are represented in multiple soil layers with

170 multiphase subsurface reactive transport. CH_4 production (i.e., acetoclastic and

171 hydrogenotrophic methanogenesis), CH_4 oxidation, and CH_4 transport (i.e., diffusion,

172 aerenchyma, and ebullition) are explicitly represented in *ecosys*. The *ecosys* model

173 operates at variable time steps (~seconds to 1 hour) determined by convergence criteria,

174 and it can be applied at patch scale (spatially homogenous one-dimensional; e.g., (Chang

175 et al., 2019a)) and landscape scale (spatially variable two- or three-dimensional; e.g.,

176 (Grant et al., 2017b, 2017a)). The *ecosys* model has been extensively examined against

177 field measurements made in 2002–2007 (Chang et al., 2019a) and 2011–2013 (Chang et

178 al., 2019b) at our study sites at the Stordalen Mire, and 2013 at our study sites at

179 Utqiagvik (Grant et al., 2017b, 2017a, 2019). A qualitative summary of the *ecosys* model

180 is provided in the supplementary material to this article, and detailed descriptions are

181 available in the supplements of (Grant et al., 2017b, 2017a). The *ecosys* model structure

182 remains unchanged from that in earlier studies.

183 **2.5 Experimental design**

184 The primary purpose of this study is to explore the implications of the observed

185 CH_4 emission hysteresis (Fig. 1) and highlight the need to recognize factors other than

186 temperature that control ecosystem-scale CH_4 emissions. We develop a mechanistic

187 explanation for such hysteresis by investigating how the modeled environmental drivers

188 modulate CH_4 emission hysteresis. The modeled data used in this study are extracted

189 from our earlier simulations that can be downloaded from the IsoGenie database

190 (https://isogenie-db.asc.ohio-state.edu/; (Chang et al., 2019a, 2019b)) and the NGEE-

191 Arctic database (https://ngee-arctic.ornl.gov/; (Chang and Riley, 2020; Grant et al.,

192 2017b, 2017a). Our analysis focuses on modeled data because some factors (e.g., root

193 exudates, substrate availability, and methanogenic population and activity) modulating

194 CH_4 production, oxidation, and emission rates are not continuously measured at our study

195 sites. Our recently published model results at the Stordalen Mire and Utqiaġvik sites

196 indicate good comparisons with observations, including for thaw depth (R^2 = 0.75 to

197 0.90), WTD (mean bias = -4.3 to 4.0 cm), and CO_2 (R^2 = 0.43 to 0.88) and CH_4 (R^2 =

198 0.31 to 0.93) surface fluxes (Chang et al., 2019a, 2019b; Grant et al., 2017b, 2017a,

199 2019). In particular, CH_4 production pathway modeled at our Stordalen Mire sites has

200 been validated by the relative abundances of acetoclastic and hydrogenotrophic

201 methanogenic lineages reported in McCalley et al. (2014), suggesting that substrate and

202 microbial dynamics are reasonably represented. For conciseness, we focus discussion in

203 the remainder of the paper on the Stordalen Mire fen site, since it exhibits strong apparent

204 hysteresis and the underlying mechanisms leading to hysteretic CH_4 emissions are similar

205 across all study sites.

206   We note the relevant point that the *ecosys* model itself represents temperature

207 dependence of soil metabolic activity and gas production through locally simulated soil

208 temperature profiles with an modified Arrhenius function that includes terms for low- and

209 high-temperature inactivation (Grant, 2015). Besides temperature effects, the *ecosys*

210 model also represents substrate controls (through Michaelis-Menten kinetics) on

211 microbial biomass and activity (e.g., Chang et al., 2019b), which is not explicitly

212 characterized by inferring an apparent whole system temperature dependence (e.g., Eq.

213 1). These representations allow the model to simulate overall CH_4 emission patterns with

214 more complex dynamics than represented in the apparent temperature dependence

215 function alone, making it a suitable tool for investigating the relative importance of

216 temperature dependence versus other factors.

217 **3. Results and discussion**

218 **3.1 Observed patterns of apparent CH_4 emission hysteresis**

219   The CH_4 emissions measured in the Stordalen Mire bog and fen exhibit

220 hysteretic responses to soil surface temperature: i.e., at the same soil surface temperature,

221 greater CH_4 emissions during the later than the earlier periods of the thawed season (Fig.

222 1). At both sites, plotting time- and chamber- specific CH_4 emission and soil surface

223 temperature measurements from the beginning to end of the thawed season results in a

224   counterclockwise hysteresis loop at each site-year (2012 to 2017). Such hysteretic

225   responses lead to intra-seasonally varying apparent CH_4 emission temperature

226   dependencies, suggesting that a proper representation of temporal variability is needed to

227   recognize factors modulating CH_4 emissions. For example, three distinct apparent CH_4

228   emission temperature dependencies can be derived from the same chamber sampling at

229   different periods within the same thawed season (i.e., earlier period, later period, and full

230   season). Despite the high spatial heterogeneity, the observed patterns of CH_4 emission

231   hysteresis are consistent across chambers within and between the bog and fen habitats.

232   Our results thus demonstrate that CH_4 emissions are generally more sensitive to

233   temperature changes during the later part of the thawed season, and that CH_4 emission

234   strength and temperature dependence vary substantially among site-years. Consistent

235   hysteretic responses can be found in CH_4 emission and air temperature measurements

236   (Supplementary Fig. 1), suggesting that the apparent CH_4 emission hysteresis is not

237   dependent on time lags between air and soil temperatures (Wohlfahrt and Galvagno,

238   2017). The observed CH_4 emission hysteresis indicates that models cannot accurately

239   represent CH_4 dynamics without representing the large spatial and temporal variability in

240   apparent CH_4 emission temperature dependencies.

241   **3.2 Modeled patterns of apparent CH_4 emission hysteresis**

242   The CH_4 emissions modeled by *ecosys*, extracted from our recently published

243   results at the Stordalen Mire and the Utqiaġvik sites (Chang et al., 2019b; Grant et al.,

244   2017b), have hysteretic responses to mean 0–20 cm soil temperature (Fig. 2) and air

245   temperature (Supplementary Fig. 2). The apparent CH_4 emission temperature dependence

246   inferred from the modeled results varies substantially from the beginning to the end of the

247   thawed season, suggesting that CH_4 emissions may not be accurately represented as a

248   single function of temperature. For each site-year, CH_4 emissions modeled in the later

249   period are greater than those in the earlier period at the same temperature (e.g., Fig. 2),

250   consistent with observations (e.g., Fig. 1). The apparent CH_4 emission hysteresis is larger

251   and clearer in the Stordalen Mire fen compared to the bog and the Utqiaġvik low-

252   centered polygon, likely from its warmer soil temperatures, shallower WTD, and higher

253   CH_4 emissions (Chang et al., 2019b). Consistent hysteresis patterns are found at weekly

254   timescales (Supplementary Fig. 4), suggesting that the apparent CH_4 emission hysteresis

255   is not sensitive to temporal resolution nor the timing of maximum seasonal temperature.

256   In addition to temporal variability, changes in biogeophysical conditions driven by fine-

257   scale hydrology and vegetation differences can also alter the apparent functional

258   relationship between CH_4 emission and temperature. For example, apparent CH_4 emission

259   temperature dependencies inferred for individual topographic features (i.e., troughs, rims,

260   and centers) vary substantially within the same wetland ecosystem at Utqiaġvik

261   (Supplementary Fig. 5).

262   We evaluate the effects of intra-seasonal variability on ecosystem-scale CH_4

263   emissions by estimating apparent CH_4 emission temperature dependencies during

264   different parts of the thawed season. By fitting the Boltzmann-Arrhenius function (Eq. 1)

265   to the CH_4 emissions and 0–20 cm soil temperatures modeled during different time

266   frames (i.e., earlier period, later period, and full season), we developed and evaluated

267   three temperature dependence models for each thawed season. Our results show that CH_4

268   emission estimates improve when apparent CH_4 emission temperature dependencies were

269   separately represented in the earlier and later periods, compared to those assuming a

270   seasonally invariant apparent CH_4 emission temperature dependence (Supplementary

271   Table 1, 2). In the Stordalen Mire, neglecting intra-seasonal variability in apparent CH_4

272   emission temperature dependence leads to overestimated (10 to 81%) and underestimated

273   (-21 to -40%) CH_4 emissions during the earlier and later periods, respectively

274   (Supplementary Table 1). Consistent prediction bias was found in the Utqiaġvik low-

275   centered polygon, except in the rims where drier conditions limit CH_4 emissions

276   (Supplementary Table 2).

277   These results demonstrate that models based on a seasonally invariant apparent

278   CH_4 emission temperature dependence may introduce errors by improperly prescribing

279   the seasonal dynamics of CH_4 biogeochemistry with a static function of temperature. The

280   substantial intra-seasonal variability, potentially led by site specific thermal and

281   hydrological history (Updegraff et al., 1998), could be an important and overlooked

282   property of natural wetlands that currently account for 25 to 32% of global total CH_4

283   emissions (Saunois et al., 2016). Representing intra-seasonally variable apparent CH_4

284   emission or production temperature dependencies in large-scale wetland biogeochemical

285   models may thus reduce CH_4 emission prediction biases and model structural uncertainty.

286   **3.3 Microbial substrate-mediated CH_4 production hysteresis**

287   For conciseness, we focus our discussion on the potential drivers causing the

288   hysteretic relationship between CH_4 emission and soil temperature modeled at the

289   Stordalen Mire fen at 2011, as the underlying mechanisms are consistent across all site-

290   years. The temporal evolution of CH_4 emissions modeled by *ecosys* follows that of CH_4

291   production, with limited offsets from CH_4 oxidation (Fig. 3a). Modeled CH_4 emission

292   (e.g., Fig. 2d) and production (Fig. 3b) rates both exhibit intra-seasonal variations in their

apparent temperature dependencies during the thawed season, consistent with the varying

temperature responses to microbial thermal history reported in laboratory incubations

(Updegraff et al., 1998). The relatively low CH_4 oxidation suggests that hysteretic

responses of modeled CH_4 emissions to temperature (Fig. 2) primarily result from

hysteretic CH_4 production (Fig. 3b) associated with asymmetric methanogen biomass

(Fig. 3c) and activity (Fig. 3d) between the earlier and later periods. Further, the

consistent seasonal cycles in CH_4 production, oxidation, and emission rates modeled

from 2011 to 2013 (Supplementary Fig. 6) indicate that the CH_4 emission hysteresis

modeled in that period (Fig. 2d, e, f) is not caused by relatively low CH_4 oxidation

modeled in a particular site-year. This result is consistent with isotopic measurements

which also indicated that changes in CH_4 production, not CH_4 oxidation, determine the

CH_4 emissions observed in the Stordalen Mire sites (McCalley et al., 2014).

Although CH_4 oxidation has been proposed to be an important control regulating

wetland CH_4 emissions, e.g., Perryman et al. (2020) and Singleton et al. (2018), the

competitive dynamics between methanogens and methanotrophs throughout the year has

not been included in such studies. The modeled CH_4 oxidation rate is relatively low

during the thawed season when CH_4 production is strongest, and relatively high during

the shoulder season when CH_4 production is weakest (Supplementary Fig. 6). These

strong seasonal variations suggest that the relative importance of CH_4 production and

oxidation on regulating CH_4 emissions may fluctuate throughout the year, highlighting

the need to properly represent the underlying dynamics controlling CH_4 biogeochemistry.

Increased soil temperatures elevate oxygen demands for aerobic heterotrophs

while reducing oxygen solubility, which favors fermenter and methanogens and thereby

316   enhance CH_4 production. Our model results indicate that the elevated methanogen

317   biomass and activity during the later period are driven by the increased substrate

318   availability for methanogenesis later in the thawed season. Specifically, modeled

319   substrate concentrations remain relatively high after peak substrate production rate at

320   maximum seasonal soil temperature for both acetoclastic (AM; Fig. 4a) and

321   hydrogenotrophic methanogenesis (HM; Fig. 5a). Relatively high AM (Fig. 4b) and HM

322   (Fig. 5b) substrate availability during the later period elevates AM and HM energy yields

323   at a given soil temperature, resulting in higher methanogen growth (Fig. 3d) and biomass

324   (Fig. 3c) later in the thawed season. Therefore, CH_4 production rates during the later

325   period become higher than those during the earlier period at the same soil temperature

326   (Fig. 3b), which drives higher CH_4 emissions with increased aqueous CH_4 concentrations.

327   Although AM and HM each exhibit microbial substrate-mediated hysteretic temperature

328   responses, AM appears to be more hysteretic to soil temperature than HM (Fig. 6). The

329   stronger AM hysteresis is consistent with the larger and clearer CH_4 emission hysteresis

330   found in the Stordalen Mire fen (Fig. 2), where the fractional contribution of AM to total

331   CH_4 production is higher than in the Stordalen Mire bog (Chang et al., 2019b; McCalley

332   et al., 2014). A schematic summarizing the above-mentioned mechanisms for microbial

333   substrate-mediated CH_4 production hysteresis is presented in Fig. 7.

334   Although the CH_4 emission rates and CH_4 production pathways modeled in the

335   Stordalen Mire fen have been examined (Chang et al., 2019b), continuous substrate

336   concentration measurements are lacking for validating the substrate-mediated hysteretic

337   temperature responses proposed here. Wide ranges of acetate and hydrogen

338   concentrations have been reported from incubation experiments studying methanogenesis

339 (e.g., Hines et al., 2008; Tøsdal et al., 2015; Zhang et al., 2020); however, those values

340 may not be used to validate the time and space specific substrate concentrations modeled

341 at our study sites. Therefore, further studies and additional field measurements are needed

342 to test our proposed hypothesis of the causes of observed CH_4 emission hysteresis.

343 **3.4 Other factors regulating intra-seasonal CH_4 emissions**

344   To evaluate whether microbial substrate-mediated CH_4 production hysteresis is

345 the primary cause of the observed hysteretic relationship between CH_4 emission and

346 temperature, we evaluated four alternative hypotheses: interactions with (1) water table

347 depth; (2) GPP (via exudation, root litter inputs, and aerenchyma development); (3) thaw

348 depth; and (4) residual pore-water CH_4 concentrations at the end of the earlier part of the

349 thawed season.

350   First, studies have found that seasonal variations of WTD determine CH_4 cycling

351 dynamics by regulating the temperature response of CH_4 emissions, leading to hysteretic

352 CH_4 emissions when drought-induced WTD drawdown below the critical zone for CH_4

353 production (Brown et al., 2014; Goodrich et al., 2015). The substantial CH_4 emission

354 hysteresis observed in the Stordalen Mire fen is unlikely caused by seasonal variations in

355 WTD, because the observed WTD are around or above the peat surface throughout the

356 thawed season with limited effects on CH_4 emissions (Bäckstrand et al., 2008b).

357   Second, Rinne et al. (2018) reported that the temporal variations of CH_4

358 emissions are strongly regulated by GPP, and the time required to convert GPP to

359 methanogenesis substrates may cause the observed apparent hysteresis found between

360 GPP and CH_4 emissions. Such apparent hysteresis was also modeled at our study sites

361 (e.g., Fig. 8a), which shows higher CH_4 emissions later in the thawed season at a given

362 GPP. We further analyzed factors linking GPP and CH_4 emissions modeled at the

363 Stordalen Mire fen to explore whether an apparent hysteretic relationship between CH_4

364 emissions and GPP is causally connected. We examined three primary pathways by

365 which GPP could lead to a delayed effect on CH_4 emissions, and thereby apparent

366 hysteresis: increases in (1) fresh carbon inputs from root exudation (Fig. 8b), (2) below-

367 ground litter inputs (Fig. 8c), and (3) aerenchyma transport caused by GPP-induced

368 growth of porous sedge roots (Fig. 8d). In contrast to the apparent hysteresis with GPP,

369 all three of these mechanisms exhibit reversed hysteresis cycles compared to those

370 between CH_4 emissions and temperature. Therefore, these three primary mechanisms are

371 inconsistent with a causal hysteretic relationship between GPP and CH_4 emissions.

372   Third, studies have suggested that soil temperature increases can expand the

373 volume of unfrozen soil and thereby stimulate deep carbon decomposition, which can

374 also contribute to higher carbon emissions later in the thawed season, as has been

375 observed for upland CO_2 emissions (Goulden et al., 1998) and wetland CH_4 emissions

376 (Iwata et al., 2015). Our results show a weak correlation between thaw depth and CH_4

377 emissions during the latter part of the thawed season, although CH_4 emissions appear to

378 increase with deeper thaw during the earlier period (Fig. 8e). Therefore, the hysteretic

379 relationship between CH_4 emission and soil temperature found at our study sites is not

380 causally connected with the greater volume of unfrozen soil later in the thawed season.

381 This result may be explained by the relatively shallow zone (mostly within the top 20 cm

382 of soil) of CH_4 production (Chang et al., 2019b) compared with the much deeper thaw

383 depth (> 90 cm) measured and modeled during the peak CH_4 emission period (i.e., July to

384 August) (Chang et al., 2019a).

385   Fourth, we conducted a sensitivity test to examine the amount of lagged CH_4

386   emissions resulting from CH_4 residual stored in the soil profile at the end of the earlier

387   part of the thawed season. In the sensitivity test, we turned off CH_4 production during the

388   later part of the thawed season so the later-period CH_4 emissions modeled in this run are

389   driven by lagged releases of earlier-period CH_4 production. At the Stordalen Mire fen,

390   later-period CH_4 emissions resulting from earlier-period CH_4 residual concentrations

391   decreased approximately exponentially and contributed about 25% of the CH_4 emissions

392   during the later period (Fig. 9). The timing and magnitude of later-period CH_4 emissions

393   attributed to lagged CH_4 emissions do not match with the relatively high CH_4 emissions

394   modeled during the later period. Therefore, our results suggest that lagged CH_4 emissions

395   from residual CH_4 produced in the earlier period are not a dominant factor leading to the

396   observed CH_4 emission hysteresis, although lagged CH_4 emissions may amplify the

397   apparent CH_4 emission hysteresis detected in the system.

398   Collectively, our results suggest that microbial substrate-mediated CH_4

399   production hysteresis is likely to be the primary control of the observed apparent CH_4

400   emission hysteresis. The physical controls on CH_4 production and emission (and

401   potentially their hysteresis patterns) in the sediments of terrestrial freshwater systems

402   may differ from those we derived from vegetated peat surfaces (Wik et al., 2016), and

403   further investigation is needed to assess their apparent temperature dependence. To better

404   understand factors controlling CH_4 production and emission, continuous measurements of

405   seasonal development of methanogenesis substrates and soil temperature at the depth

406   where CH_4 production is prevalent are needed.

407   **4. Conclusions**

408   Many contemporary CH_4 models parameterize wetland CH_4 production (or

409   emission) as a fixed fraction of net primary productivity or heterotrophic respiration

410   regulated by a single static function of temperature (Melton et al., 2013; Wania et al.,

411   2013). Our results suggest that such a parameterization is not accurate because it

412   oversimplifies microbial responses to changing thermal and hydrological conditions that

413   modulate wetland CH_4 production and emission rates. More continuous observations

414   across sites are required to assess model prediction uncertainty and the broader extent to

415   which our mechanistic explanations apply. In summary, we found that apparent CH_4

416   emission temperature dependencies vary from the earlier to later part of the thawed

417   season due to substrate-mediated CH_4 production hysteresis caused by intra-seasonal

418   changes in methanogen biomass and activity. We examined four alternative mechanisms

419   that may contribute to the observed CH_4 emission hysteresis with temperature, and found

420   none of them can exclusively explain the underlying dynamics. Our findings motivate

421   explicit model representations of microbial dynamics that physiologically link microbial

422   and abiotic interactions, as only three of 40 recently reviewed CH_4 models

423   mechanistically represent CH_4 biogeochemistry (Xu et al., 2016).

424   **Code availability**

425   The *ecosys* source code is available at Zenodo (doi:10.5281/zenodo.3906642).

426   **Data availability**

427   The data presented in this study are available at the NGEE Arctic Database

428   (doi:10.5440/1635534).

429   **Author contribution**

430   KYC and WJR designed the study. PMC synthesized field measurements and RFG

431   developed the *ecosys* model. KYC performed the analyses and led the writing of the

432   paper. All authors contributed thoughtful discussions and insights to the study, and all

433   authors contributed to the editing of the paper.

434   **Competing interests**

435   The authors declare that they have no conflict of interest.

436   **Acknowledgements**

437   This study was funded by the Genomic Science Program of the United States

438   Department of Energy Office of Biological and Environmental Research under the

439   ISOGENIE (DE-SC0016440) and NGEE-Arctic projects under contract DE-AC02-

440   05CH11231 to Lawrence Berkeley National Laboratory and grants from Swedish VR

441   (Vetenskaprådet) and Swedish FORMAS to PMC. We acknowledge US National

442   Science Foundation MacroSystems program (NSF EF 1241037) support for

443   autochamber measurements between 2013 and 2017. We thank the Abisko Scientific

444   Research Station of the Swedish Polar Research Secretariat for providing the

445   meteorological data.

446   **References**

447   Bäckstrand, K., Crill, P. M., Mastepanov, M., Christensen, T. R. and Bastviken, D.: Non-

448   methane volatile organic compound flux from a subarctic mire in Northern Sweden,

449   Tellus, Ser. B Chem. Phys. Meteorol., doi:10.1111/j.1600-0889.2007.00331.x, 2008a.

450   Bäckstrand, K., Crill, P. M., Mastepanov, M., Christensen, T. R. and Bastviken, D.: Total

451   hydrocarbon flux dynamics at a subarctic mire in northern Sweden, J. Geophys. Res.

452   Biogeosciences, doi:10.1029/2008JG000703, 2008b.

453 Bäckstrand, K., Crill, P. M., Jackowicz-Korczyñski, M., Mastepanov, M., Christensen, T.

454 R. and Bastviken, D.: Annual carbon gas budget for a subarctic peatland, Northern

455 Sweden, Biogeosciences, 7(1), 95–108, doi:10.5194/bg-7-95-2010, 2010.

456 Bastviken, D., Tranvik, L. J., Downing, J. A., Crill, P. M. and Enrich-Prast, A.:

457 Freshwater methane emissions offset the continental carbon sink, Science (80-.).,

458 331(6013), 50, doi:10.1126/science.1196808, 2011.

459 Biskaborn, B. K., Smith, S. L., Noetzli, J., Matthes, H., Vieira, G., Streletskiy, D. A.,

460 Schoeneich, P., Romanovsky, V. E., Lewkowicz, A. G., Abramov, A., Allard, M., Boike, J.,

461 Cable, W. L., Christiansen, H. H., Delaloye, R., Diekmann, B., Drozdov, D., Etzelmüller,

462 B., Grosse, G., Guglielmin, M., Ingeman-Nielsen, T., Isaksen, K., Ishikawa, M.,

463 Johansson, M., Johannsson, H., Joo, A., Kaverin, D., Kholodov, A., Konstantinov, P.,

464 Kröger, T., Lambiel, C., Lanckman, J. P., Luo, D., Malkova, G., Meiklejohn, I.,

465 Moskalenko, N., Oliva, M., Phillips, M., Ramos, M., Sannel, A. B. K., Sergeev, D.,

466 Seybold, C., Skryabin, P., Vasiliev, A., Wu, Q., Yoshikawa, K., Zheleznyak, M. and

467 Lantuit, H.: Permafrost is warming at a global scale, Nat. Commun., 10(1), 1–11,

468 doi:10.1038/s41467-018-08240-4, 2019.

469 Brown, M. G., Humphreys, E. R., Moore, T. R., Roulet, N. T. and Lafleur, P. M.: Evidence

470 for a nonmonotonic relationship between ecosystem-scale peatland methane

471 emissions and water table depth, J. Geophys. Res. Biogeosciences, 119(5), 826–835,

472 doi:10.1002/2013JG002576, 2014.

473 Bubier, J., Crill, P., Mosedale, A., Frolking, S. and Linder, E.: Peatland responses to

474 varying interannual moisture conditions as measured by automatic CO 2 chambers ,

475 Global Biogeochem. Cycles, doi:10.1029/2002gb001946, 2003.

476 Chang, K.-Y. and Riley, W.: Hysteretic temperature sensitivity of wetland CH4 fluxes

477 explained by substrate availability and microbial activity: Model Archive, Next

478 Gener. Ecosyst. Exp. Arct. Data Collect. Oak Ridge Natl. Lab. U.S. Dep. Energy, Oak

479 Ridge, Tennessee, USA, doi:10.5440/1635534, 2020.

480 Chang, K.-Y., Riley, W. J., Crill, P. M., Grant, R. F., Rich, V. I. and Saleska, S. R.: Large

481 carbon cycle sensitivities to climate across a permafrost thaw gradient in subarctic

482 Sweden, Cryosph., 13(2), 647–663, doi:10.5194/tc-13-647-2019, 2019a.

483 Chang, K.-Y., Riley, W. J., Brodie, E. L., McCalley, C. K., Crill, P. M. and Grant, R. F.:

484 Methane Production Pathway Regulated Proximally by Substrate Availability and

485 Distally by Temperature in a High-Latitude Mire Complex, J. Geophys. Res.

486 Biogeosciences, 2019JG005355, doi:10.1029/2019JG005355, 2019b.

487 Ciais, P., Sabine, C., Bala, G., Bopp, L., Brovkin, V., Canadell, J., Chhabra, A., DeFries, R.,

488 Galloway, J., Heimann, M., Jones, C., Quéré, C. Le, Myneni, R. B., Piao, S. and Thornton,

489 P.: Carbon and Other Biogeochemical Cycles, in Climate Change 2013 - The Physical

490 Science Basis, edited by Stocker, T.F., D. Qin, G.-K. Plattner, M. Tignor, S. K. Allen, J.

491 Boschung, A. Nauels, Y. Xia, V. Bex, and P. M. Midgley, pp. 465–570, Cambridge

492 University Press, Cambridge, United Kingdom and New York, NY, USA, Cambridge.,

493 2013.

494 Dean, J. F., Middelburg, J. J., Röckmann, T., Aerts, R., Blauw, L. G., Egger, M., Jetten, M.

495 S. M., de Jong, A. E. E., Meisel, O. H., Rasigraf, O., Slomp, C. P., in't Zandt, M. H. and

496 Dolman, A. J.: Methane Feedbacks to the Global Climate System in a Warmer World,

497 Rev. Geophys., 56(1), 207–250, doi:10.1002/2017RG000559, 2018.

498 Eyring, V., Bony, S., Meehl, G. A., Senior, C. A., Stevens, B., Stouffer, R. J. and Taylor, K.

499   E.: Overview of the Coupled Model Intercomparison Project Phase 6 (CMIP6)

500   experimental design and organization, Geosci. Model Dev., 9(5), 1937–1958,

501   doi:10.5194/gmd-9-1937-2016, 2016.

502   Goodrich, J. P., Campbell, D. I., Roulet, N. T., Clearwater, M. J. and Schipper, L. A.:

503   Overriding control of methane flux temporal variability by water table dynamics in a

504   Southern Hemisphere, raised bog, J. Geophys. Res. Biogeosciences, 120(5), 819–831,

505   doi:10.1002/2014JG002844, 2015.

506   Goulden, M. L., Wofsy, S. C., Harden, J. W., Trumbore, S. E., Crill, P. M., Gower, S. T.,

507   Fries, T., Daube, B. C., Fan, S.-M., Sutton, D. J., Bazzaz, A. and Munger, J. W.: Sensitivity

508   of Boreal Forest Carbon Balance to Soil Thaw, Science (80-.)., 279(5348), 214–217,

509   doi:10.1126/science.279.5348.214, 1998.

510   Grant, R. F.: Ecosystem CO_2 and CH_4 exchange in a mixed tundra and a fen within a

511   hydrologically diverse Arctic landscape: 2. Modeled impacts of climate change, J.

512   Geophys. Res. Biogeosciences, 120(7), 1388–1406, doi:10.1002/2014JG002889,

513   2015.

514   Grant, R. F., Mekonnen, Z. A., Riley, W. J., Wainwright, H. M., Graham, D. and Torn, M.

515   S.: Mathematical Modelling of Arctic Polygonal Tundra with Ecosys: 1.

516   Microtopography Determines How Active Layer Depths Respond to Changes in

517   Temperature and Precipitation, J. Geophys. Res. Biogeosciences, 122(12), 3161–

518   3173, doi:10.1002/2017JG004035, 2017a.

519   Grant, R. F., Mekonnen, Z. A., Riley, W. J., Arora, B. and Torn, M. S.: Mathematical

520   Modelling of Arctic Polygonal Tundra with Ecosys: 2. Microtopography Determines

521   How CO_2 and CH_4 Exchange Responds to Changes in Temperature and

522   Precipitation, J. Geophys. Res. Biogeosciences, 122(12), 3174–3187,

523   doi:10.1002/2017JG004037, 2017b.

524   Grant, R. F., Mekonnen, Z. A., Riley, W. J., Arora, B. and Torn, M. S.: Modelling climate

525   change impacts on an Arctic polygonal tundra. Part 2: Changes in CO_2 and CH_4

526   exchange depend on rates of permafrost thaw as affected by changes in vegetation

527   and drainage, J. Geophys. Res. Biogeosciences, 2018JG004645,

528   doi:10.1029/2018JG004645, 2019.

529   Hemes, K. S., Chamberlain, S. D., Eichelmann, E., Knox, S. H. and Baldocchi, D. D.: A

530   Biogeochemical Compromise: The High Methane Cost of Sequestering Carbon in

531   Restored Wetlands, Geophys. Res. Lett., 45(12), 6081–6091,

532   doi:10.1029/2018GL077747, 2018.

533   Hines, M. E., Duddleston, K. N., Rooney-Varga, J. N., Fields, D. and Chanton, J. P.:

534   Uncoupling of acetate degradation from methane formation in Alaskan wetlands:

535   Connections to vegetation distribution, Global Biogeochem. Cycles, 22(2), n/a-n/a,

536   doi:10.1029/2006GB002903, 2008.

537   Hinkel, K. M., Frohn, R. C., Nelson, F. E., Eisner, W. R. and Beck, R. A.: Morphometric

538   and spatial analysis of thaw lakes and drained thaw lake basins in the western Arctic

539   Coastal Plain, Alaska, Permafr. Periglac. Process., doi:10.1002/ppp.532, 2005.

540   Hodgkins, S. B., Tfaily, M. M., McCalley, C. K., Logan, T. A., Crill, P. M., Saleska, S. R.,

541   Rich, V. I. and Chanton, J. P.: Changes in peat chemistry associated with permafrost

542   thaw increase greenhouse gas production, Proc. Natl. Acad. Sci.,

543   doi:10.1073/pnas.1314641111, 2014.

544   Iwata, H., Harazono, Y., Ueyama, M., Sakabe, A., Nagano, H., Kosugi, Y., Takahashi, K.

545 and Kim, Y.: Methane exchange in a poorly-drained black spruce forest over

546 permafrost observed using the eddy covariance technique, Agric. For. Meteorol.,

547 214–215, 157–168, doi:10.1016/j.agrformet.2015.08.252, 2015.

548 Kirschke, S., Bousquet, P., Ciais, P., Saunois, M., Canadell, J. G., Dlugokencky, E. J.,

549 Bergamaschi, P., Bergmann, D., Blake, D. R., Bruhwiler, L., Cameron-Smith, P.,

550 Castaldi, S., Chevallier, F., Feng, L., Fraser, A., Heimann, M., Hodson, E. L., Houweling,

551 S., Josse, B., Fraser, P. J., Krummel, P. B., Lamarque, J.-F., Langenfelds, R. L., Le Quéré,

552 C., Naik, V., O'Doherty, S., Palmer, P. I., Pison, I., Plummer, D., Poulter, B., Prinn, R. G.,

553 Rigby, M., Ringeval, B., Santini, M., Schmidt, M., Shindell, D. T., Simpson, I. J., Spahni,

554 R., Steele, L. P., Strode, S. A., Sudo, K., Szopa, S., van der Werf, G. R., Voulgarakis, A.,

555 van Weele, M., Weiss, R. F., Williams, J. E. and Zeng, G.: Three decades of global

556 methane sources and sinks, Nat. Geosci., 6(10), 813–823, doi:10.1038/ngeo1955,

557 2013.

558 Knoblauch, C., Beer, C., Liebner, S., Grigoriev, M. N. and Pfeiffer, E. M.: Methane

559 production as key to the greenhouse gas budget of thawing permafrost, Nat. Clim.

560 Chang., 1–4, doi:10.1038/s41558-018-0095-z, 2018.

561 Malmer, N., Johansson, T., Olsrud, M. and Christensen, T. R.: Vegetation, climatic

562 changes and net carbon sequestration in a North-Scandinavian subarctic mire over

563 30 years, Glob. Chang. Biol., doi:10.1111/j.1365-2486.2005.01042.x, 2005.

564 McCalley, C. K., Woodcroft, B. J., Hodgkins, S. B., Wehr, R. A., Kim, E.-H., Mondav, R.,

565 Crill, P. M., Chanton, J. P., Rich, V. I., Tyson, G. W. and Saleska, S. R.: Methane

566 dynamics regulated by microbial community response to permafrost thaw, Nature,

567 514(7523), 478–481, doi:10.1038/nature13798, 2014.

568 Melton, J. R., Wania, R., Hodson, E. L., Poulter, B., Ringeval, B., Spahni, R., Bohn, T.,

569 Avis, C. A., Beerling, D. J., Chen, G., Eliseev, A. V., Denisov, S. N., Hopcroft, P. O.,

570 Lettenmaier, D. P., Riley, W. J., Singarayer, J. S., Subin, Z. M., Tian, H., Zürcher, S.,

571 Brovkin, V., van Bodegom, P. M., Kleinen, T., Yu, Z. C. and Kaplan, J. O.: Present state

572 of global wetland extent and wetland methane modelling: conclusions from a model

573 inter-comparison project (WETCHIMP), Biogeosciences, 10(2), 753–788,

574 doi:10.5194/bg-10-753-2013, 2013.

575 Myhre, G., D., Shindell, F.-M., Bréon, Collins, W., Fuglestvedt, J., Huang, J., Koch, D.,

576 Lamarque, J.-F., D. Lee, Mendoza, B., Nakajima, T., A. Robock, G. Stephens, Takemura,

577 T. and Zhang, H.: Anthropogenic and Natural Radiative Forcing, in Climate Change

578 2013 - The Physical Science Basis, vol. 23, edited by Intergovernmental Panel on

579 Climate Change, pp. 659–740, Cambridge University Press, Cambridge., 2013.

580 Neubauer, S. C. and Megonigal, J. P.: Moving Beyond Global Warming Potentials to

581 Quantify the Climatic Role of Ecosystems, Ecosystems, 18(6), 1000–1013,

582 doi:10.1007/s10021-015-9879-4, 2015.

583 Olefeldt, D. and Roulet, N. T.: Effects of permafrost and hydrology on the

584 composition and transport of dissolved organic carbon in a subarctic peatland

585 complex, J. Geophys. Res. Biogeosciences, 117(1), 1–15,

586 doi:10.1029/2011JG001819, 2012.

587 Olefeldt, D., Turetsky, M. R., Crill, P. M. and Mcguire, A. D.: Environmental and

588 physical controls on northern terrestrial methane emissions across permafrost

589 zones, Glob. Chang. Biol., 19(2), 589–603, doi:10.1111/gcb.12071, 2013.

590 Perryman, C. R., McCalley, C. K., Malhotra, A., Fahnestock, M. F., Kashi, N. N., Bryce, J.

591   G., Giesler, R. and Varner, R. K.: Thaw Transitions and Redox Conditions Drive

592   Methane Oxidation in a Permafrost Peatland, J. Geophys. Res. Biogeosciences,

593   125(3), doi:10.1029/2019JG005526, 2020.

594   Poulter, B., Bousquet, P., Canadell, J. G., Ciais, P., Peregon, A., Saunois, M., Arora, V. K.,

595   Beerling, D. J., Brovkin, V., Jones, C. D., Joos, F., Gedney, N., Ito, A., Kleinen, T., Koven,

596   C. D., McDonald, K., Melton, J. R., Peng, C., Peng, S., Prigent, C., Schroeder, R., Riley, W.

597   J., Saito, M., Spahni, R., Tian, H., Taylor, L., Viovy, N., Wilton, D., Wiltshire, A., Xu, X.,

598   Zhang, B., Zhang, Z. and Zhu, Q.: Global wetland contribution to 2000–2012

599   atmospheric methane growth rate dynamics, Environ. Res. Lett., 12(9), 094013,

600   doi:10.1088/1748-9326/aa8391, 2017.

601   Rinne, J., Tuittila, E. S., Peltola, O., Li, X., Raivonen, M., Alekseychik, P., Haapanala, S.,

602   Pihlatie, M., Aurela, M., Mammarella, I. and Vesala, T.: Temporal Variation of

603   Ecosystem Scale Methane Emission From a Boreal Fen in Relation to Temperature,

604   Water Table Position, and Carbon Dioxide Fluxes, Global Biogeochem. Cycles, 32(7),

605   1087–1106, doi:10.1029/2017GB005747, 2018.

606   Rydén, B. E. and Kostov, L.: Thawing and Freezing in Tundra Soils, Ecol. Bull., (30),

607   251–281 [online] Available from: http://www.jstor.org/stable/20112776, 1980.

608   Saunois, M., Bousquet, P., Poulter, B., Peregon, A., Ciais, P., Canadell, J. G.,

609   Dlugokencky, E. J., Etiope, G., Bastviken, D., Houweling, S., Janssens-Maenhout, G.,

610   Tubiello, F. N., Castaldi, S., Jackson, R. B., Alexe, M., Arora, V. K., Beerling, D. J.,

611   Bergamaschi, P., Blake, D. R., Brailsford, G., Brovkin, V., Bruhwiler, L., Crevoisier, C.,

612   Crill, P., Covey, K., Curry, C., Frankenberg, C., Gedney, N., Höglund-Isaksson, L.,

613   Ishizawa, M., Ito, A., Joos, F., Kim, H. S., Kleinen, T., Krummel, P., Lamarque, J. F.,

614   Langenfelds, R., Locatelli, R., Machida, T., Maksyutov, S., McDonald, K. C., Marshall, J.,

615   Melton, J. R., Morino, I., Naik, V., O'Doherty, S., Parmentier, F. J. W., Patra, P. K., Peng,

616   C., Peng, S., Peters, G. P., Pison, I., Prigent, C., Prinn, R., Ramonet, M., Riley, W. J., Saito,

617   M., Santini, M., Schroeder, R., Simpson, I. J., Spahni, R., Steele, P., Takizawa, A.,

618   Thornton, B. F., Tian, H., Tohjima, Y., Viovy, N., Voulgarakis, A., Van Weele, M., Van

619   Der Werf, G. R., Weiss, R., Wiedinmyer, C., Wilton, D. J., Wiltshire, A., Worthy, D.,

620   Wunch, D., Xu, X., Yoshida, Y., Zhang, B., Zhang, Z. and Zhu, Q.: The global methane

621   budget 2000-2012, Earth Syst. Sci. Data, 8(2), 697–751, doi:10.5194/essd-8-697-

622   2016, 2016.

623   Saunois, M., Bousquet, P., Poulter, B., Peregon, A., Ciais, P., Canadell, J. G.,

624   Dlugokencky, E. J., Etiope, G., Bastviken, D., Houweling, S., Janssens-Maenhout, G.,

625   Tubiello, F. N., Castaldi, S., Jackson, R. B., Alexe, M., Arora, V. K., Beerling, D. J.,

626   Bergamaschi, P., Blake, D. R., Brailsford, G., Bruhwiler, L., Crevoisier, C., Crill, P.,

627   Covey, K., Frankenberg, C., Gedney, N., Höglund-Isaksson, L., Ishizawa, M., Ito, A.,

628   Joos, F., Kim, H. S., Kleinen, T., Krummel, P., Lamarque, J. F., Langenfelds, R., Locatelli,

629   R., Machida, T., Maksyutov, S., Melton, J. R., Morino, I., Naik, V., O'Doherty, S.,

630   Parmentier, F. J. W., Patra, P. K., Peng, C., Peng, S., Peters, G. P., Pison, I., Prinn, R.,

631   Ramonet, M., Riley, W. J., Saito, M., Santini, M., Schroeder, R., Simpson, I. J., Spahni, R.,

632   Takizawa, A., Thornton, B. F., Tian, H., Tohjima, Y., Viovy, N., Voulgarakis, A., Weiss,

633   R., Wilton, D. J., Wiltshire, A., Worthy, D., Wunch, D., Xu, X., Yoshida, Y., Zhang, B.,

634   Zhang, Z. and Zhu, Q.: Variability and quasi-decadal changes in the methane budget

635   over the period 2000-2012, Atmos. Chem. Phys., 17(18), 11135–11161,

636   doi:10.5194/acp-17-11135-2017, 2017.

637 Schuur, E. A. G., McGuire, A. D., Schädel, C., Grosse, G., Harden, J. W., Hayes, D. J.,

638 Hugelius, G., Koven, C. D., Kuhry, P., Lawrence, D. M., Natali, S. M., Olefeldt, D.,

639 Romanovsky, V. E., Schaefer, K., Turetsky, M. R., Treat, C. C. and Vonk, J. E.: Climate

640 change and the permafrost carbon feedback, Nature, 520(7546), 171–179,

641 doi:10.1038/nature14338, 2015.

642 Shiklomanov, N. I., Streletskiy, D. A., Nelson, F. E., Hollister, R. D., Romanovsky, V. E.,

643 Tweedie, C. E., Bockheim, J. G. and Brown, J.: Decadal variations of active-layer

644 thickness in moisture-controlled landscapes, Barrow, Alaska, J. Geophys. Res.

645 Biogeosciences, doi:10.1029/2009JG001248, 2010.

646 Singleton, C. M., McCalley, C. K., Woodcroft, B. J., Boyd, J. A., Evans, P. N., Hodgkins, S.

647 B., Chanton, J. P., Frolking, S., Crill, P. M., Saleska, S. R., Rich, V. I. and Tyson, G. W.:

648 Methanotrophy across a natural permafrost thaw environment, ISME J., 12(10),

649 2544–2558, doi:10.1038/s41396-018-0065-5, 2018.

650 Tang, J. and Riley, W. J.: Weaker soil carbon-climate feedbacks resulting from

651 microbial and abiotic interactions, Nat. Clim. Chang., advance on(January),

652 doi:10.1038/nclimate2438, 2014.

653 Tøsdal, A., Urich, T., Frenzel, P. and Marianne, M.: Metabolic and trophic interactions

654 modulate methane production by Arctic peat microbiota in response to warming,

655 Proc. Natl. Acad. Sci., E2507–E2516, doi:10.1073/pnas.1420797112, 2015.

656 Updegraff, K., Bridgham, S. D., Pastor, J. and Weishampel, P.: Hysteresis in the

657 temperature response of carbon dioxide and methane production in peat soils,

658 Biogeochemistry, 43(3), 253–272, doi:10.1023/A:1006097808262, 1998.

659 Wainwright, H. M., Dafflon, B., Smith, L. J., Hahn, M. S., Curtis, J. B., Wu, Y., Ulrich, C.,

660   Peterson, J. E., Torn, M. S. and Hubbard, S. S.: Identifying multiscale zonation and

661   assessing the relative importance of polygon geomorphology on carbon fluxes in an

662   Arctic tundra ecosystem, J. Geophys. Res. Biogeosciences,

663   doi:10.1002/2014JG002799, 2015.

664   Wania, R., Melton, J. R., Hodson, E. L., Poulter, B., Ringeval, B., Spahni, R., Bohn, T.,

665   Avis, C. A., Chen, G., Eliseev, A. V., Hopcroft, P. O., Riley, W. J., Subin, Z. M., Tian, H.,

666   Van Bodegom, P. M., Kleinen, T., Yu, Z. C., Singarayer, J. S., Zürcher, S., Lettenmaier, D.

667   P., Beerling, D. J., Denisov, S. N., Prigent, C., Papa, F. and Kaplan, J. O.: Present state of

668   global wetland extent and wetland methane modelling: Methodology of a model

669   inter-comparison project (WETCHIMP), Geosci. Model Dev., 6(3), 617–641,

670   doi:10.5194/gmd-6-617-2013, 2013.

671   Wik, M., Varner, R. K., Anthony, K. W., MacIntyre, S. and Bastviken, D.: Climate-

672   sensitive northern lakes and ponds are critical components of methane release, Nat.

673   Geosci., 9(2), 99–105, doi:10.1038/ngeo2578, 2016.

674   Wohlfahrt, G. and Galvagno, M.: Revisiting the choice of the driving temperature for

675   eddy covariance CO2flux partitioning, Agric. For. Meteorol., 237–238, 135–142,

676   doi:10.1016/j.agrformet.2017.02.012, 2017.

677   Xu, X., Yuan, F., Hanson, P. J., Wullschleger, S. D., Thornton, P. E., Riley, W. J., Song, X.,

678   Graham, D. E., Song, C. and Tian, H.: Reviews and syntheses: Four decades of

679   modeling methane cycling in terrestrial ecosystems, Biogeosciences, 13(12), 3735–

680   3755, doi:10.5194/bg-13-3735-2016, 2016.

681   Yvon-Durocher, G., Allen, A. P., Bastviken, D., Conrad, R., Gudasz, C., St-Pierre, A.,

682   Thanh-Duc, N. and Del Giorgio, P. A.: Methane fluxes show consistent temperature

683   dependence across microbial to ecosystem scales, Nature, 507(7493), 488–491,

684   doi:10.1038/nature13164, 2014.

685   Zhang, L., Liu, X., Duddleston, K. and Hines, M. E.: The Effects of pH, Temperature,

686   and Humic-Like Substances on Anaerobic Carbon Degradation and Methanogenesis

687   in Ombrotrophic and Minerotrophic Alaskan Peatlands, Aquat. Geochemistry,

688   (0123456789), doi:10.1007/s10498-020-09372-0, 2020.

689   Zona, D., Gioli, B., Commane, R., Lindaas, J., Wofsy, S. C. and Miller, C. E.: Cold season

690   emissions dominate the Arctic tundra methane budget, Proc. Natl. Acad. Sci., 113(1),

691   40–45, doi:10.1073/pnas.1516017113, 2016.

692

693
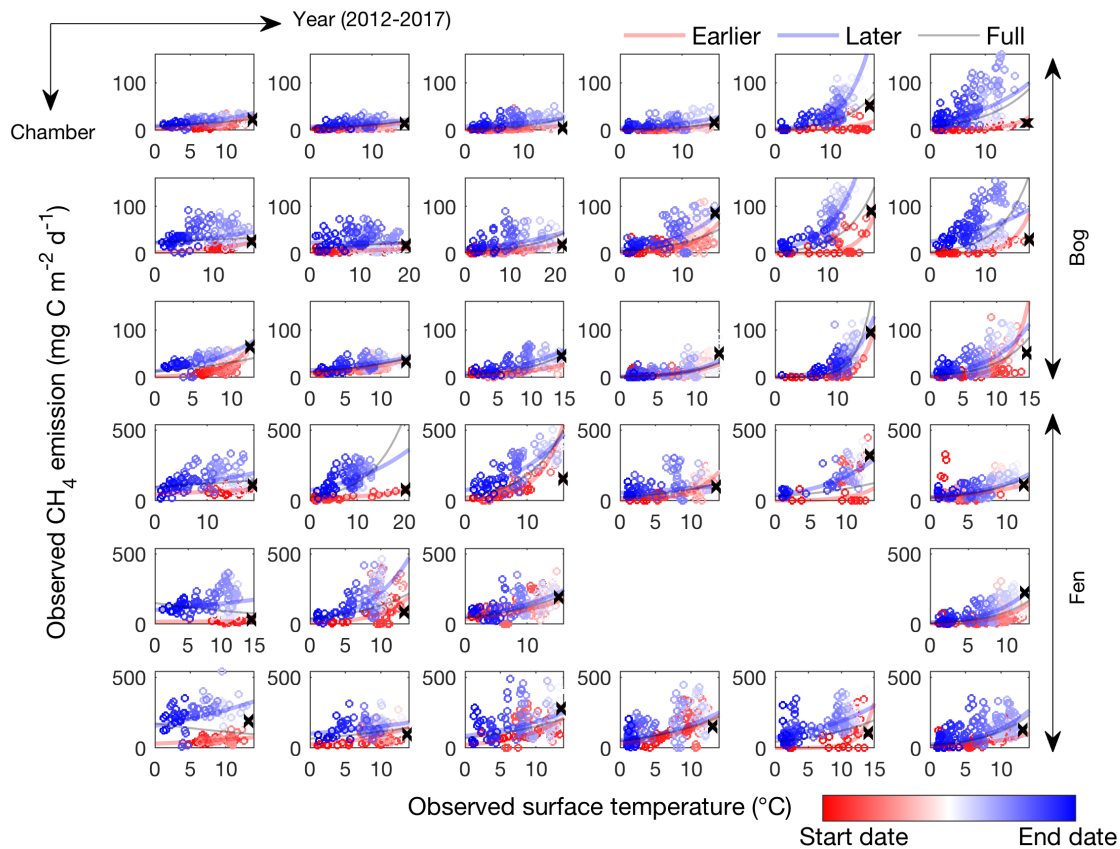
Figure 1. CH4 emissions are hysteretic to soil surface temperature measured in individual

automated chambers at the Stordalen Mire bog (top three panels) and fen (bottom three

panels) sites from 2012 to 2017 thawed seasons (left to right). Open circles and lines

represent the daily data points and the fitted apparent CH4 emission temperature

dependence, respectively. The earlier, later, and full-season periods are colored in red,

blue, and black, respectively. Earlier and later periods are defined as the time before and

after the seasonal maximum soil surface temperature denoted by black cross signs. Start

date and end dates represent the beginning and ending of a thawed season defined as the

period when measured daily soil surface temperature is above 1 ˚C, respectively.

703

704
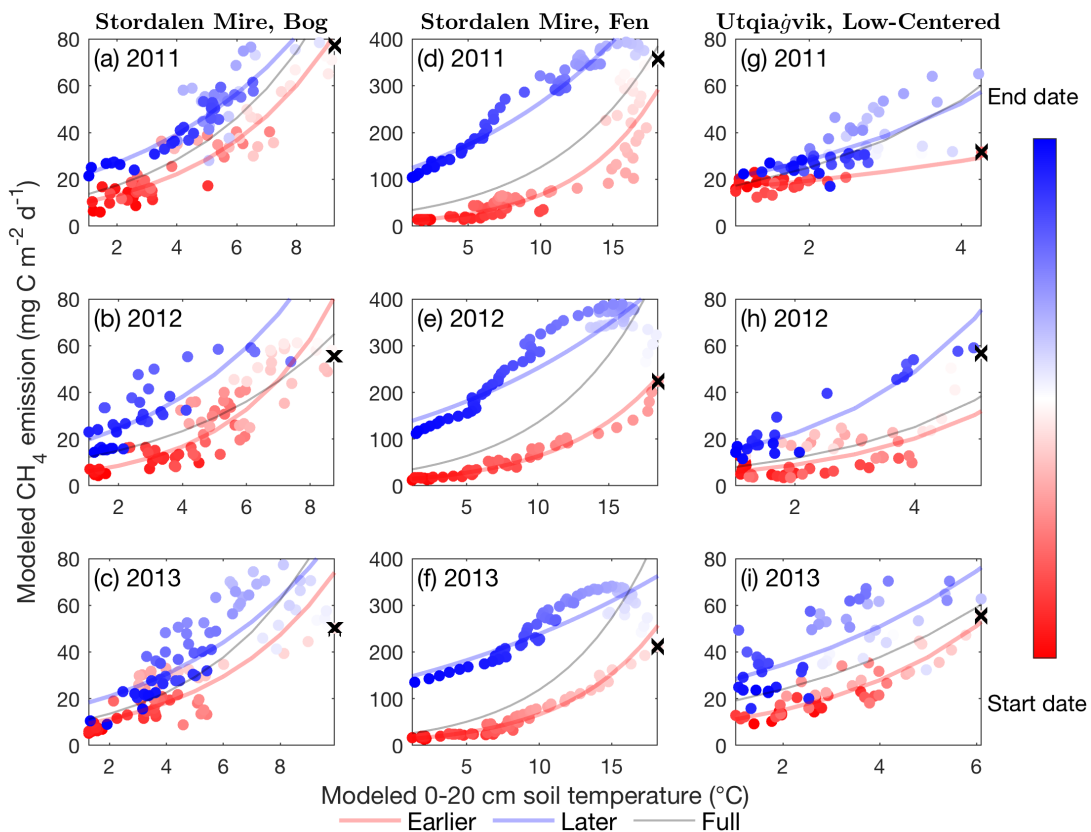
Figure 2. CH4 emissions are hysteretic to soil temperature modeled in the Stordalen Mire

bog (a to c) and fen (d to f) and the Utqiaġvik low-centered polygon (g to i) from 2011 to

2013 thawed seasons. Dots and lines represent the daily data points and the fitted

apparent temperature dependence, respectively. Earlier, later, and full-season periods are

colored in red, blue, and black, respectively. Earlier and later periods are defined as the

time before and after the seasonal maximum 0-20 cm soil temperature denoted by black

cross signs. Start date and end dates represent the beginning and ending of a thawed

season defined as the period when modeled daily 0-20 cm soil temperature is above 1 ˚C,

respectively.

714

715
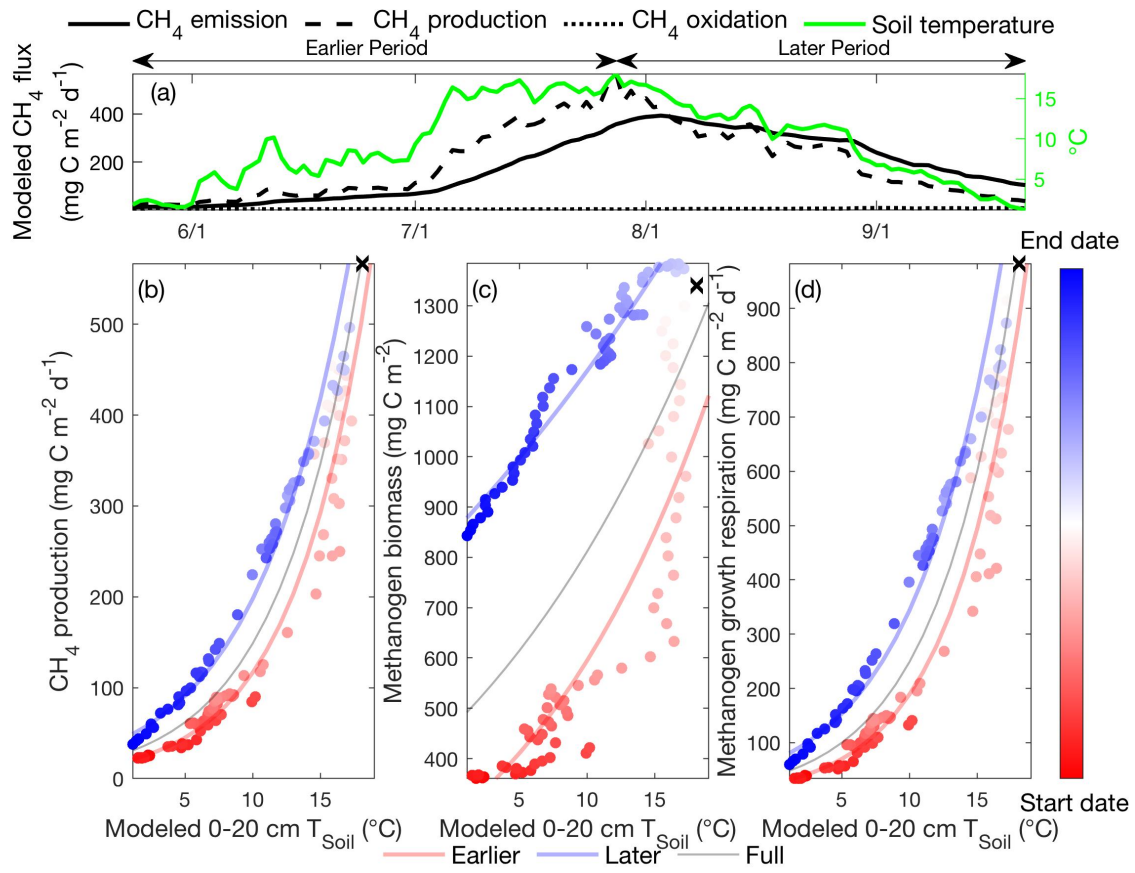
Figure 3. Intra-seasonal variations in apparent CH_4 production temperature dependence

result from asymmetric microbial biomass and activity modeled between the earlier and

later periods. Daily CH_4 emissions, CH_4 production, CH_4 oxidation, and 0-20 cm soil

temperature modeled in the Stordalen Mire fen during the 2011 thawed season (a). The

corresponding apparent temperature dependence of the modeled CH_4 production (b),

methanogen biomass (c), and methanogen growth respiration (d) during the 2011 thawed

season. Earlier, later, and full-season periods are colored in red, blue, and black,

respectively. Earlier and later periods are defined as the time before and after the seasonal

maximum 0-20 cm soil temperature denoted by black cross signs. Start date and end

dates represent the beginning and ending of a thawed season defined as the period when

modeled daily 0-20 cm soil temperature is above 1 ˚C, respectively.

727
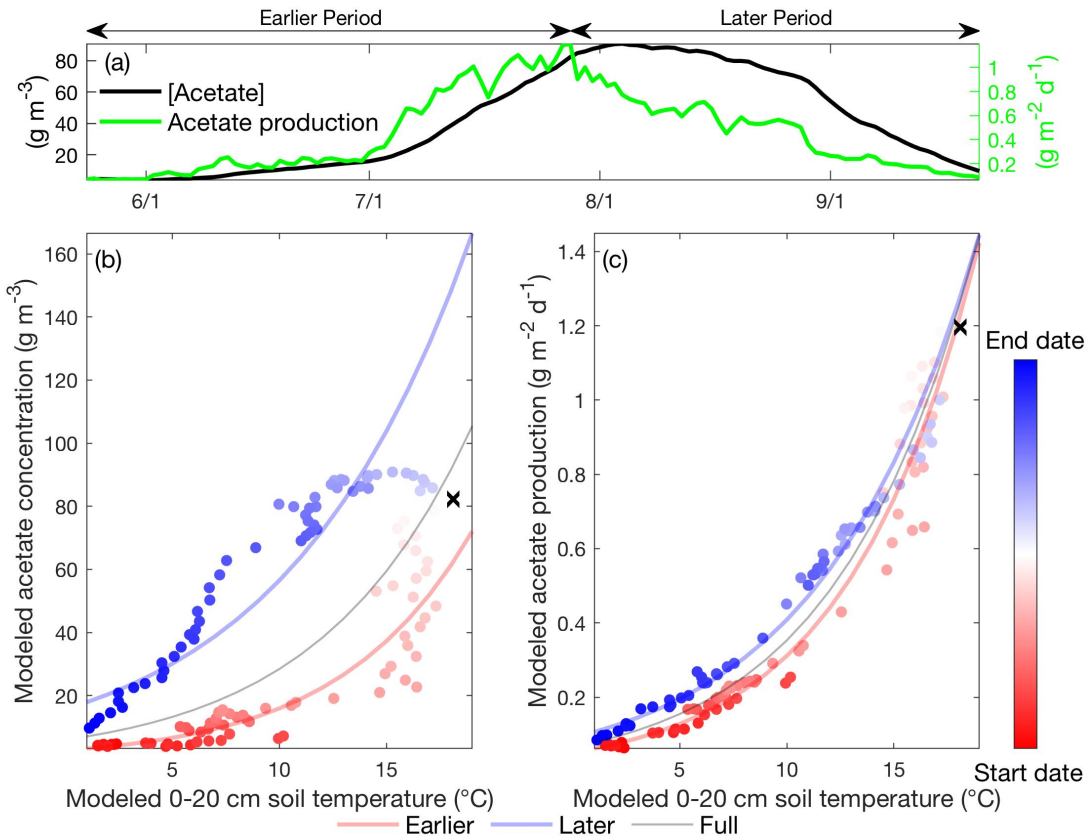
728

729 Figure 4. Daily acetate concentration and acetate production modeled in the Stordalen

730 Mire fen during the 2011 thawed season (a). The corresponding apparent temperature

731 dependence of the modeled acetate concentration (b) and acetate production (c) during

732 the 2011 thawed season. Dots and lines represent the daily data points and the fitted

733 apparent temperature dependence, respectively. The earlier, later, and full-season periods

734 are colored in red, blue, and black, respectively. Earlier and later periods are defined as

735 the time before and after the seasonal maximum 0-20 cm soil temperature denoted by

736 black cross signs. Start date and end dates represent the beginning and ending of a thawed

737 season defined as the period when modeled daily 0-20 cm soil temperature is above 1 ˚C,

738 respectively.

739
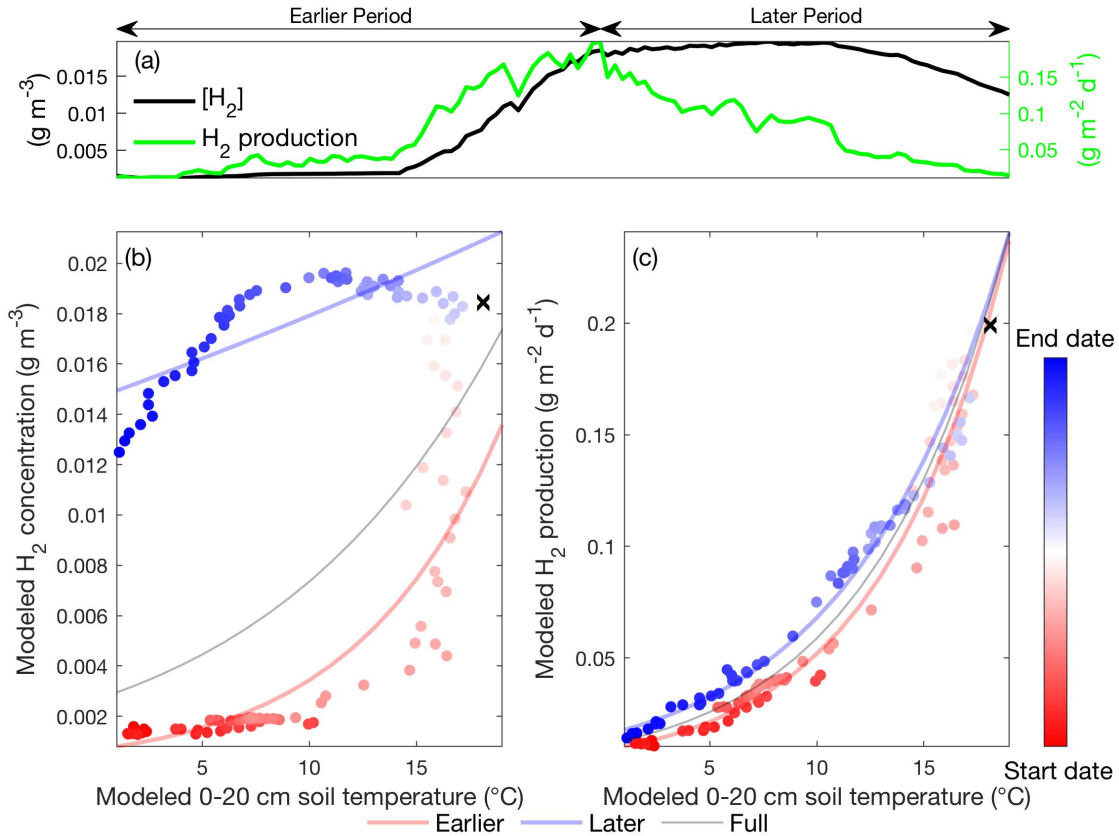
740

741 Figure 5. Daily hydrogen concentration and hydrogen production modeled in the

742 Stordalen Mire fen during the 2011 thawed season (a). The corresponding apparent

743 temperature dependence of the modeled hydrogen concentration (b) and hydrogen

744 production (c) during the 2011 thawed season. Dots and lines represent the daily data

745 points and the fitted apparent temperature dependence, respectively. The earlier, later,

746 and full-season periods are colored in red, blue, and black, respectively. Earlier and later

747 periods are defined as the time before and after the seasonal maximum 0-20 cm soil

748 temperature denoted by black cross signs. Start date and end dates represent the

749 beginning and ending of a thawed season defined as the period when modeled daily 0-20

750 cm soil temperature is above 1 ˚C, respectively.

751

752
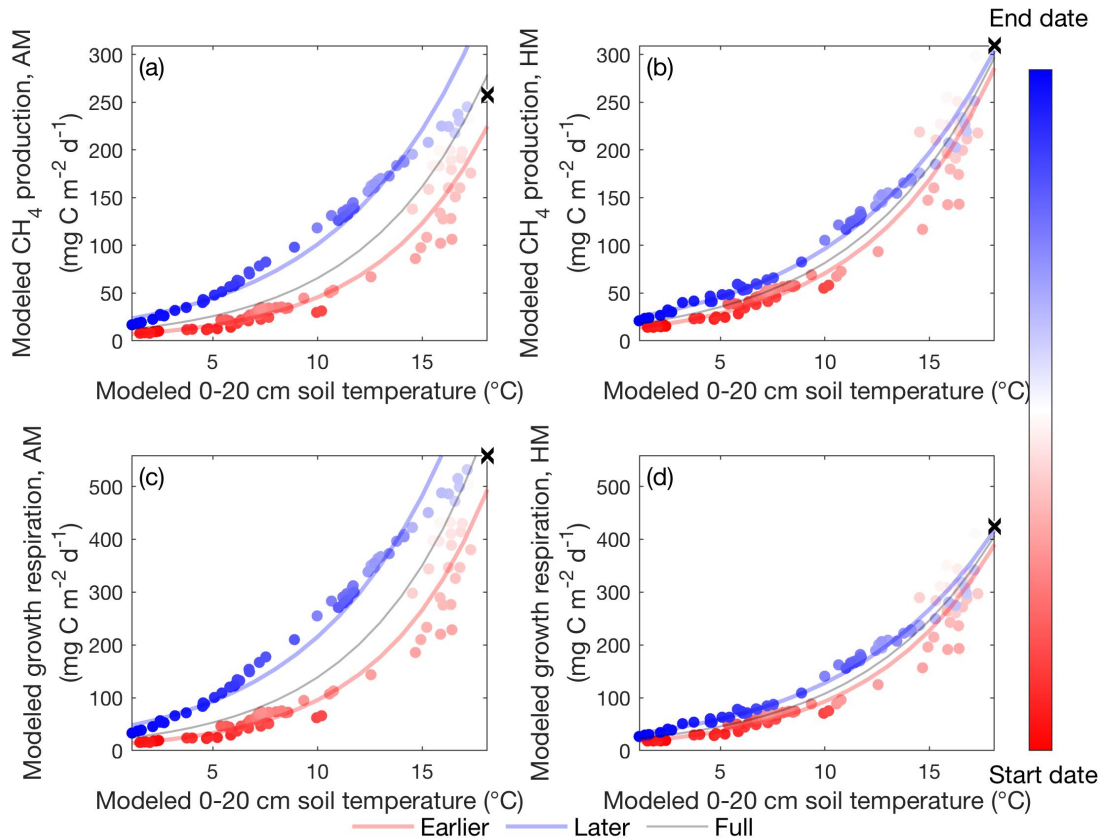
Figure 6. Apparent temperature dependence of daily CH_4 production for acetoclastic (a)

and hydrogenotrophic (b) methanogenesis, and daily growth respiration for acetoclastic

(c) and hydrogenotrophic (d) methanogens modeled in the Stordalen Mire fen during the

2011 thawed season. Dots and lines represent the daily data points and the fitted apparent

temperature dependence, respectively. The earlier, later, and full-season periods are

colored in red, blue, and black, respectively. Earlier and later periods are defined as the

time before and after the seasonal maximum 0-20 cm soil temperature denoted by black

cross signs. Start date and end dates represent the beginning and ending of a thawed

season defined as the period when modeled daily 0-20 cm soil temperature is above 1 ˚C,

respectively.

763
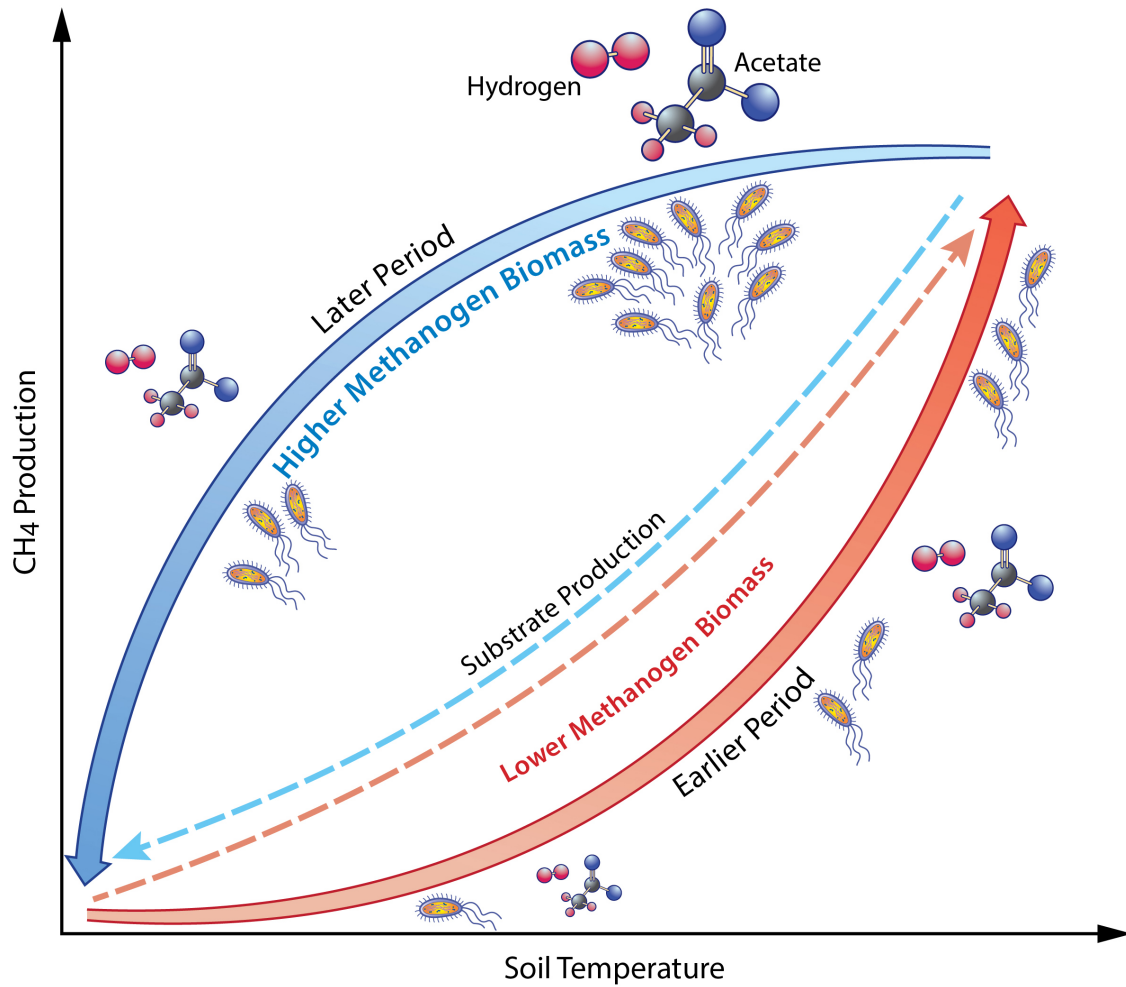
Figure 7. Schematic of the microbial substrate-mediated CH_4 production hysteresis

proposed in this study. Higher substrate (i.e., acetate and hydrogen) availability

stimulates higher methanogen biomass during the later period, which leads to intra-

seasonal differences in CH_4 production between the earlier and later periods.

768
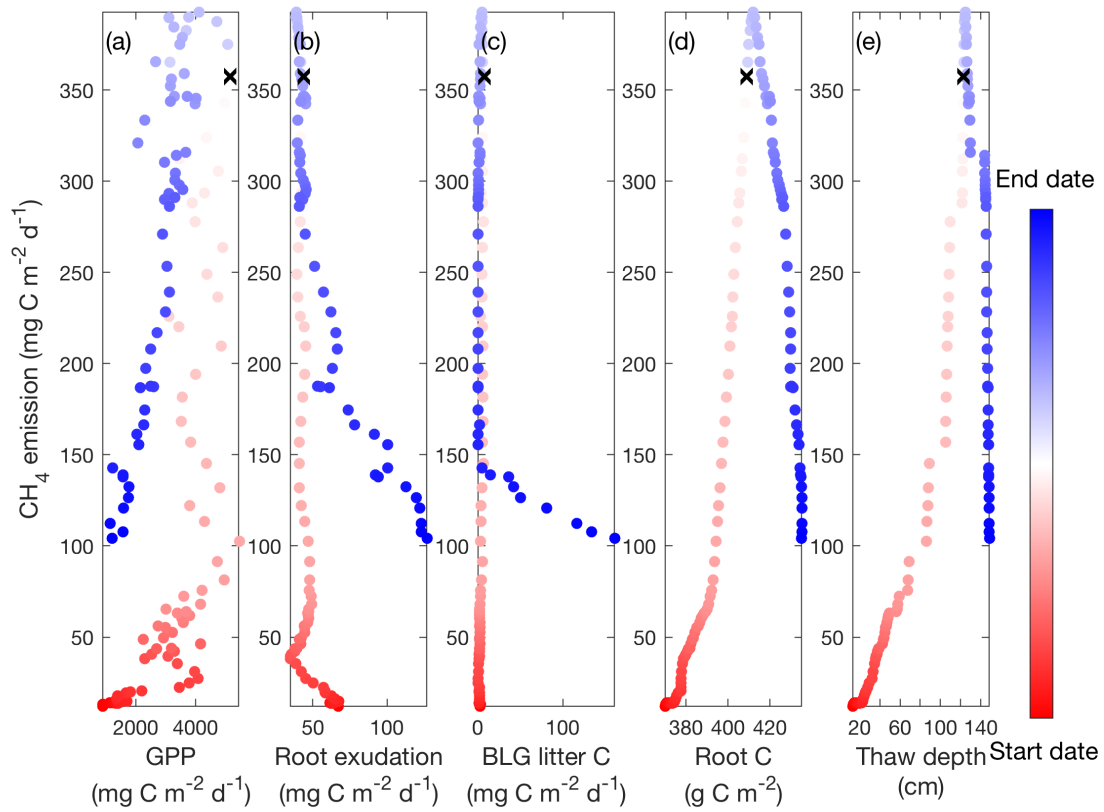
769

770 Figure 8. Daily CH$_4$ emissions have hysteretic responses to gross primary productivity

771 (a), carbon released from root exudation (b), carbon released from belowground litter

772 decomposition (c), the amount of root biomass for sedges (d), and thaw depth (e)

773 modeled in the Stordalen Mire fen during the 2011 thawed season. Dots and lines

774 represent the daily data points and the fitted apparent temperature dependence,

775 respectively. Black cross signs represent the seasonal maximum 0-20 cm soil

776 temperature. Start date and end dates represent the beginning and ending of a thawed

777 season defined as the period when modeled daily 0-20 cm soil temperature is above 1 ˚C,

778 respectively.

779
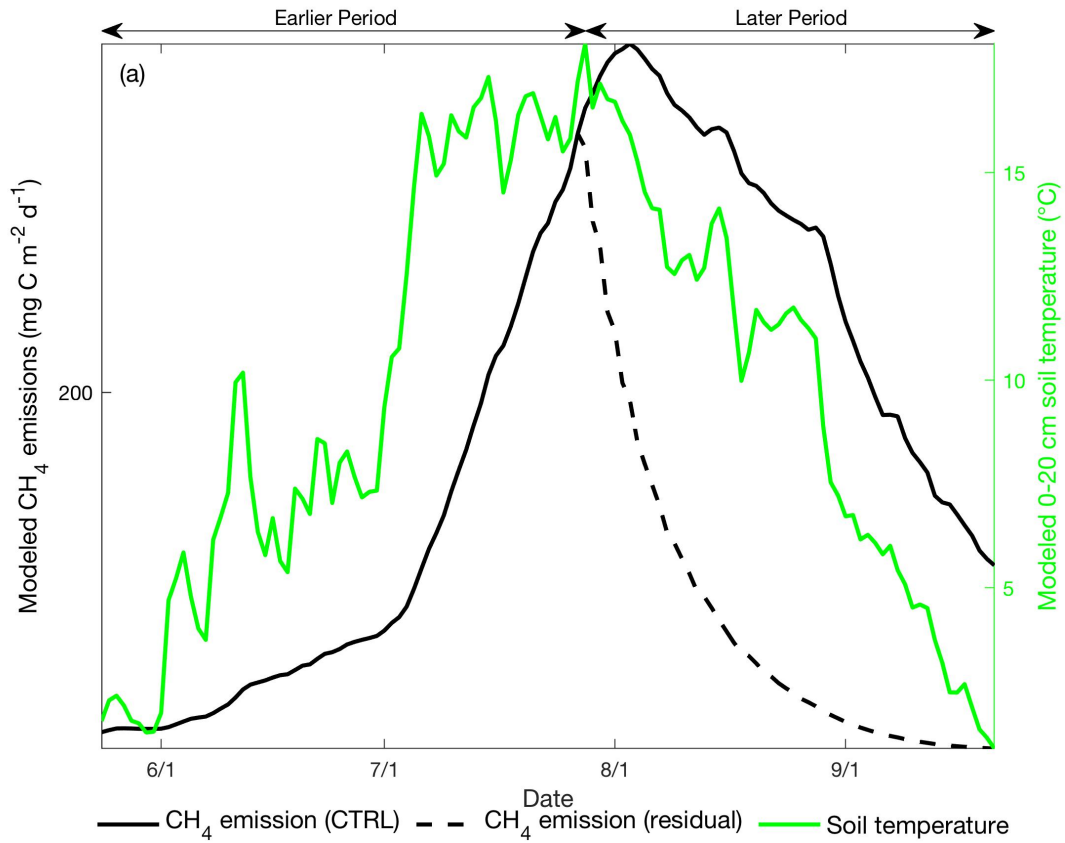
780

781 Figure 9. Daily CH$_4$ emissions (black line, left axis) and 0-20 cm mean soil temperature

782 (green line, right axis) modeled at the Stordalen Mire fen during the 2011 thawed season.

783 Black solid and dashed lines represent the modeled CH$_4$ emissions with and without CH$_4$

784 production during the later period, respectively. Earlier and later periods are defined as

785 the time before and after the modeled seasonal maximum 0-20 cm soil temperature.

786

787